Nanoscale

RSC Publishing

PAPER

View Article Online
View Journal | View Issue

Cite this: *Nanoscale*, 2013, **5**, 12356

Inorganic nanoparticle multilayers using photo-crosslinking layer-by-layer assembly and their applications in nonvolatile memory devices

Sanghyuk Cheong,†[a] Younghoon Kim,†[a] Taegyun Kwon,[b] Bumjoon J. Kim[b] and Jinhan Cho*[a]

Received 26th August 2013
Accepted 2nd October 2013

DOI: 10.1039/c3nr04547a

www.rsc.org/nanoscale

We introduce a general and facile method for the preparation of organic/inorganic nanoparticle (NP) nanocomposite multilayer films that allows vertical growth of various NP layers (*i.e.*, metal or transition metal oxide NPs) in a densely packed structure. Our approach is based on the successive photo-crosslinking layer-by-layer (LbL) assembly between hydrophobic ligands onto a NP surface and photoinitiator (PI) molecules. Therefore, our approach requires neither the additional surface modification needed for well-defined NPs synthesized in organic media nor the deposition step that inserts a polymer layer bridge between adjacent inorganic NP layers in the preparation of traditional LbL-assembled NP films. We also demonstrate that photo-crosslinking LbL-assembled (metal oxide NP)$_n$ films could be used as a nonvolatile memory layer without a high-temperature thermal treatment, unlike conventional vacuum-deposition- or sol–gel-derived memory devices, which require thermal treatments at temperatures greater than 200 °C. This robust method could open a facile route for the design of functional NP-based electronic devices.

1. Introduction

Organic/inorganic nanocomposite films based on functional metal or metal oxide nanoparticles (NPs) have attracted considerable attention due to their potential applications in electrochemical sensors, optical display films, supercapacitors, photovoltaic films, memory devices, gas barrier films, mechanically reinforced films, *etc*.[1–10] Although a variety of approaches to the preparation of nanocomposite films have been introduced, such as blending,[11] sol–gel processes,[12] the self-assembly of block copolymers,[13] and the molecular recognition method,[14] the layer-by-layer (LbL) assembly method[15–28] is potentially the most versatile and offers diverse opportunities for the preparation of organic/inorganic NP hybrid films.

An important advantage of this method is that it enables the preparation of nanocomposite films with a tailored film thickness, chemical composition, functionality, and internal structure on substrates. In addition, a variety of functional materials can be inserted within LbL films through complementary interactions (*i.e.*, electrostatic, hydrogen bonding, click chemistry, disulfide bonding, silanization, urethane linking, and amidation) in polar solvents—mainly aqueous media.[15–24,26,28] Recent progress in LbL assembly has allowed the successive adsorption of functional components in nonpolar solvents such as toluene or hexane by covalent bonding between successively deposited polymer and inorganic materials.[25,27,29–31] LbL-assembly in organic media may increase the number of adsorbed inorganic NPs per layer over that of the conventional electrostatic LbL-assembly, which forms loosely packed NP layers due to electrostatic repulsion between equally charged NPs in aqueous media.[32,33]

For most applications, functional inorganic NPs should be of good quality, including a uniform size and high degree of crystallinity. The synthesis of inorganic NPs in organic media is more desirable than their synthesis in aqueous media. The highest-quality inorganic NPs can be easily synthesized using unsaturated fatty acid stabilizers, such as oleic acid (OA), in organic media.[34,35] In addition, the inorganic NP-based LbL films prepared in organic solvents can be effectively applied to data storage devices such as memory devices, whereas the diffused or residual moisture within films prepared in aqueous media can cause the malfunction of electronic devices and/or a high level of leakage current.

However, despite the previously discussed notable advantages, LbL approaches based on a dipping process in aqueous or organic media require the adsorption of desired NPs and polymers *via* a self-diffusion process, followed by rinsing of weakly adsorbed NPs and polymers; therefore, they are not appropriate for the build-up of multilayers composed of only

[a]*Department of Chemical and Biological Engineering, Korea University, Anam-dong, Seongbuk-gu, Seoul 136-713, Korea. E-mail: jinhan71@korea.ac.kr; Fax: +82 2 926 6102; Tel: +82 2 3290 4852*

[b]*Department of Chemical and Biomolecular Engineering, Korea Advanced Institute of Science and Technology, Daejeon 305-701, Korea*

† These authors equally contributed to this work.

one kind of NP layer without the insertion of additional polymer layers. Furthermore, the inorganic NPs used in traditional LbL assembly should be stabilized by selective and limited organic ligands, and the polymers should have functional moieties with high affinities for the ligands bound to the surface of the inorganic NPs. Considering that the feasibility of device construction and applications based on LbL-assembly has been limited by the chemical complexity of material synthesis and the thin film processing difficulty, it is critical to develop an approach by which a variety of hydrophobic NPs synthesized in organic media can be easily LbL assembled without the additional ligand exchange and/or polymers while a highly uniform and homogeneous internal structure is simultaneously induced.

Herein, we introduce a general and facile approach for the preparation of LbL-assembled multilayers with a high packing density of well-defined NPs. Our methodology is based on the photo-crosslinking LbL assembly between 1-hydroxycyclohexyl phenyl ketone (HPK) as a photoinitiator (PI) molecule and OA-stabilized NPs (OA–Ag, OA–FePt, OA–MnO, and OA–Fe_3O_4). The repetitive processes of photo-crosslinking and spin-coating lead to formation of a crosslinked and highly packed NP layer without the additional surface modification required of pristine inorganic NPs (*i.e.*, OA–NPs) for complementary interactions. Although our group has previously reported that fluorescent quantum dots (QDs) can be encapsulated by hydrophobic polymers with UV-crosslinkable azide units and thiol moieties and then deposited by UV-crosslinking and spin-coating, these photo-crosslinkable polymers were synthesized *via* relatively complex steps and could not be used for the surface modification of transition metal oxide NPs. Furthermore, the approaches using a solution mixture of polymers and inorganic NPs exhibited the segregation phenomenon by which a simple spin-coating process induces two distinct layers composed of residual polymers and polymer-coated QD NPs because of their unfavorable interfacial interaction.[36] Therefore, these approaches are not suitable for the preparation of memory devices requiring the uniformly distributed charge trap elements within the films.

However, our current approach, which is based on a photo-crosslinking reaction between PI molecules and OA ligands, can form homogeneously distributed NPs within films and can therefore be effectively used for electronic applications, such as the fabrication of nonvolatile memory devices. For demonstrating this possibility, the multilayer films composed of OA–Fe_3O_4 NPs were prepared on Pt-coated substrates using the photo-crosslinking and spin-LbL assembly method, and then a tungsten tip as a top electrode was made to directly come into contact with the (crosslinked Fe_3O_4 NP)$_n$ multilayer films to measure the electrical properties. When an external bias was applied to the 6-layered devices, a switching phenomenon depending on the voltage polarity (*i.e.*, bipolar switching) was observed at low operating voltages (RESET at −1.8 V and SET voltage at +1.5 V), fast switching speed in the nanosecond level, and ON/OFF current ratio of $\sim 10^3$. Particularly, it is demonstrated that the ON/OFF current ratio of devices increases from 10^1 to 10^4 with increasing the film thickness from 20 to 80 nm although one Fe_3O_4 NP of about 6 nm size can be operated as a nanoscale-memory device. Furthermore, it should be noted that the Fe_3O_4 film with a thickness of above 40 nm and a smooth surface could not be obtained from single step spin-coating, and the resultant single layered device was not suitable for high performance memory devices.

For more evidently demonstrating the effectiveness of photo-crosslinking LbL-assembly, it is also demonstrated that the crosslinked OA–Fe_3O_4 NP memory devices with patterned Ag electrodes can be prepared using the deposition and successive photo-crosslinking of the OA–Ag NP layer without an aid of vacuum deposition. Although the vacuum deposition of top electrodes onto the nanoporous film such as OA–Fe_3O_4 NP films often gives rise to the short circuit current phenomenon, our approach based on the crosslinked Ag NP layer can reduce the short circuit current phenomenon significantly. Therefore, we believe that our approach can provide a basis for exploiting and designing a variety of organic/inorganic nanocomposite films with tailored functionalities as well as nonvolatile memory devices because inorganic NPs with compositions that range from metal to transition metal oxide can be easily incorporated into LbL multilayer films.

2. Experimental section

Synthesis of OA–Fe_3O_4 NPs

OA-stabilized Fe_3O_4 of about 6 nm was synthesized in toluene as reported previously by Sun *et al.*[34] $Fe(acac)_3$ (2 mmol, Aldrich), 1,2-hexadecanediol (10 mmol, Aldrich), OA (5 mmol, Aldrich), oleylamine (6 mmol, Aldrich), and benzyl ether (20 mL, Aldrich) were mixed and stirred under a flow of nitrogen. The mixture was heated to 200 °C for 2 h and heated to reflux (about 300 °C) for 1 h under a blanket of nitrogen. The black-colored mixture was cooled to room temperature by removing the heat source. Ethanol (40 mL) was added to the mixture under ambient conditions and a black material was precipitated and separated *via* centrifugation. The black product was dissolved in hexane in the presence of OA (0.05 mL) and oleyamine (0.05 mL). Centrifugation (6000 rpm, 10 min) was performed to remove any undispersed residue. A black-brown hexane or toluene dispersion of 6 nm Fe_3O_4 NPs was produced.

Synthesis of OA–Ag NPs

OA (2.8 g, Aldrich) was dissolved in triethylamine (40 mL, Aldrich) followed by addition of $AgNO_3$ (1.8 g, Aldrich). After 10 min of stirring, the solution turned into white slurry which was refluxed at 80 °C for 2 h. The synthesized Ag NPs were purified twice by adding acetone (40 mL) followed by centrifugation at 3500 rpm for 5 min. These Ag NPs were dried under vacuum, and then dispersed in toluene.[37]

Synthesis of OA–MnO NPs

MnO NPs were prepared according to the synthetic procedure reported by Na *et al.*[38] Manganese chloride tetrahydrate ($MnCl_2 \cdot 4H_2O$, 40 mmol) and sodium oleate (80 mmol) were added to a mixture composed of ethanol (30 mL), distilled water

(40 mL), and *n*-hexane (70 mL). The solution was heated to 70 °C and then incubated overnight at this temperature. After that, the formed Mn–oleate complex (1.24 g, 2 mmol) was dissolved in 1-octadecene (10 g). The mixture solution was kept at 70 °C for 1 hour under vacuum to eliminate water and oxygen. Then, the solution was heated up to 300 °C for 1 hour. After heating, the mixture solution was cooled to room temperature, and the formed MnO NPs were redispersed in hexane or toluene.

Synthesis of OA–FePt NPs

FePt NPs with a diameter of about 7 nm were synthesized as previously reported by Chen *et al.*[39] Briefly, a mixture of 0.5 mmol of $Pt(acac)_2$, 10 mL of benzyl ether, and 5 mL of octadecene was heated to 60 °C under nitrogen. The mixture solution was further heated to 120 °C. $Fe(CO)_5$ (0.2 mmol) and oleic acid (5 mmol) were introduced and after 5 minutes, oleylamine (5 mmol) was added. The mixture solution was then heated up to 205 °C and incubated at this temperature for 2 hours. After heating, the solution was cooled down to room temperature.

Build-up of photocrosslinked multilayers

The mixture of OA–inorganic NPs (5 mg mL^{-1}) and 1-hydroxycyclohexyl phenyl ketone (HPK) (3 wt%, Aldrich) was prepared in toluene. For spin-assembled multilayer films, the mixture solution was completely wetted on the amine-functionalized polymer-coated quartz or silicon substrates. The substrate was then rotated with a spinner at 3000 rpm for 20 s and the resulting films were photo-crosslinked under UV irradiation ($\lambda = 254$ nm) for about 20 min. After photo-crosslinking, the weakly adsorbed OA–Fe_3O_4 NPs were removed using a washing solvent (*i.e.*, pure toluene). The next layers were also sequentially deposited onto the previous films using the same procedure. These processes were repeated up to desired deposition cycles.

Fourier transform infrared (FTIR) spectroscopy

Vibrational spectra were obtained by FTIR spectroscopy (iS10 FT-IR, Thermo Fisher) in the transmission and attenuated total reflection (ATR) modes. The sample chamber was purged with N_2 gas for 2 h to eliminate water and CO_2 prior to conducting the FTIR measurement. ATR-FTIR spectra for OA, HPK, and a mixture of OA and HPK deposited onto a Au-coated substrate were obtained from 200 scans with an incident angle of 80°. The acquired raw data were plotted after baseline correction, and the spectrum was smoothed using spectrum analyzing software (OMNIC, Nicolet).

Quartz crystal microgravimetry (QCM) measurements

A QCM device (QCM200, SRS) was used to examine the mass of the material deposited after each adsorption step as previously reported.[40] The resonance frequency of the QCM electrodes was approximately 5 MHz. The adsorbed mass of hydrophobic NPs and HPK Δm was calculated from the change in QCM frequency, ΔF, using the Sauerbrey equation:

$$\Delta F(\mathrm{Hz}) = -\frac{2{F_0}^2}{A\sqrt{\rho_q \mu_q}}\Delta m$$

Here, F_0 (~5 MHz) is the fundamental resonance frequency of the crystal, A is the electrode area, and ρ_q, (~2.65 g cm^{-2}) and μ_q (~2.95×10^{11} g cm^{-2} s^{-2}) are the shear modulus and density of quartz, respectively. This equation can be simplified as follows:

$$\Delta F(\mathrm{Hz}) = -56.6 \times \Delta m_A,$$

$\Delta F(\mathrm{Hz}) = -56.6 \times \Delta m_A$, where Δm_A is the mass change per quartz crystal unit area in μg cm^{-2}.

Fabrication of resistive switching memory devices

All the samples were prepared on Si substrates (2 cm × 2 cm) with a SiO_2 layer. The bottom electrode (Pt) with 100 nm thickness was deposited onto Si substrates using a DC-magnetron sputtering system. The (crosslinked OA–Fe_3O_4)$_{n=2,4,\text{ and }6}$ multilayer films were then formed on the Pt-coated Si substrates. The resistive switching memory properties of the resultant Fe_3O_4 NP multilayer films were investigated using a tungsten electrode with 50 μm diameter without any additional thermal treatment. To investigate the resistive switching behavior of LbL multilayered devices, the current–voltage (*I–V*) curves were measured using a semiconductor parametric analyzer (SPA, Agilent 4155B) in the air environment. The pulsed voltage duration dependence of high and low current states was investigated using a semiconductor parametric analyzer (HP 4155A) and a pulse generator (Agilent 81104A) in the laboratory environment.

3. Results and discussion

To prepare photo-crosslinkable inorganic NP multilayer films, we first synthesized 0.5 wt% oleic acid (OA)-stabilized Fe_3O_4 NPs with a diameter of approximately 6 nm in toluene solution (Fig. 1a); 3 wt% 1-hydroxycyclohexyl phenyl ketone (HPK), which could be photo-crosslinked with OA ligands that contain double bonds under UV irradiation ($\lambda = 254$ nm), was subsequently added to the OA–Fe_3O_4 NP solution. The crosslinking reaction between HPK and OA ligands was confirmed by Fourier-transform infrared (FTIR) spectroscopy; specifically, the crosslinking was confirmed by the disappearance of absorbance peaks associated with C=C–H stretching (3005 cm^{-1}) in the OA ligands (Fig. 1b). In addition, the intensities of the absorbance peaks (*i.e.*, C=C–C (1577 and 1597 cm^{-1}) and C=C–H stretching (3064 cm^{-1})) associated with the benzene ring of HPK significantly decreased due to the photoinitiation and propagation of HPK by UV irradiation. UV irradiation of the reaction mixture for approximately 20 min resulted in the formation of a stable layer that was not removed when washed with the same solvent.

On the basis of these results, we investigated the vertical growth of crosslinked OA–Fe_3O_4 NP multilayers (using a 0.5 wt% OA–Fe_3O_4 NP solution) through consecutive

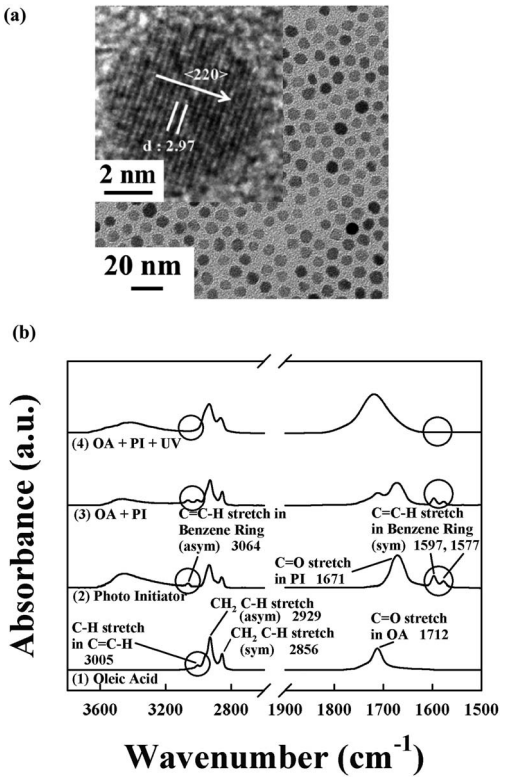

Fig. 1 (a) HR-TEM image of 6 nm sized OA–Fe_3O_4 NPs. (b) FTIR absorption spectra of OA ligands, HPK photoinitiator, and the OA–HPK mixture before and after UV light irradiation ($\lambda = 254$ nm).

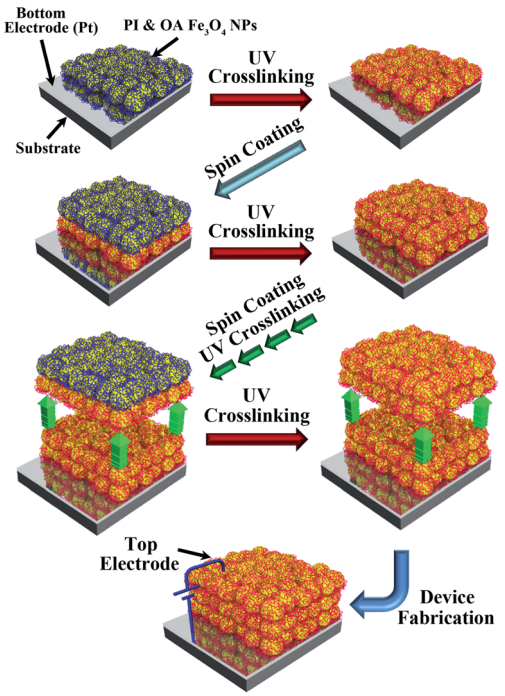

Scheme 1 Schematic representation of LbL growth of photo-crosslinked OA–Fe_3O_4 NP multilayer films.

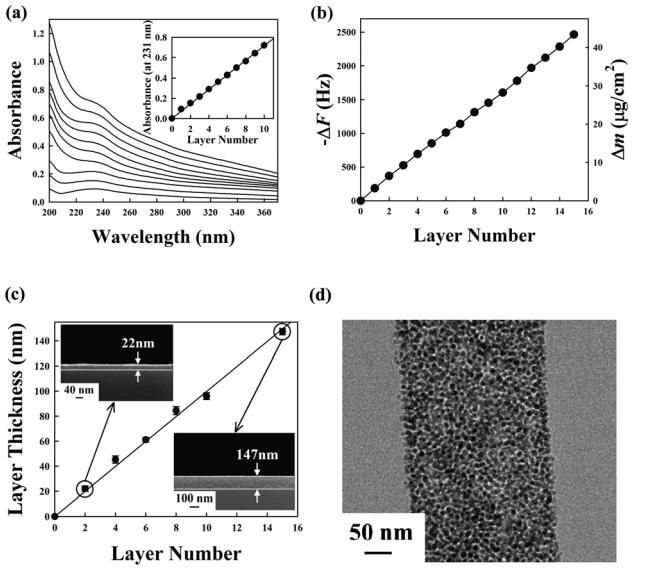

Fig. 2 (a) UV-vis spectra, (b) QCM data, (c) film thickness, and (d) cross-sectional HR-TEM image of (photo-crosslinked OA–Fe_3O_4 NP)$_n$ multilayers as a function of number of layers (n). The inset of (c) indicates the tilted SEM image of multilayers.

spin-coating and photo-crosslinking (Scheme 1). The uniform increase in absorbance implies that the fabrication process can lead to the regular growth of a multilayer film without the necessity of complementary interactions (Fig. 2a). Furthermore, the growth of the (OA–Fe_3O_4 NP)$_n$ multilayers was quantitatively monitored through the use of quartz-crystal microgravimetry (QCM) (Fig. 2b). The highly regular changes in the QCM frequency ($-\Delta F$) or mass (Δm) corresponding to the increase in number of layers (n) clearly demonstrate the LbL growth of a (OA–Fe_3O_4 NP)$_n$ multilayer film. Specifically, the deposition of each layer of OA–Fe_3O_4 NPs resulted in a $-\Delta F$ of approximately 164 Hz per layer, which corresponds to a Δm value of approximately 2.9 μg cm^{-2}. The mass changes were calculated from the frequency changes using the Sauerbrey equation.

When the QCM electrode spin-coated with a Fe_3O_4 NP layer was thermally annealed in nitrogen at 450 °C, the organic components, including the OA ligands and HPK, were completely eliminated from the film, and the $-\Delta F$ per pure Fe_3O_4 layer was measured to be approximately 80 Hz (Δm approximately 1.39 μg cm^{-2}). Given that the adsorbed mass, density, and diameter of a Fe_3O_4 NP are 1.39 μg cm^{-2}, 5.17 g cm^{-3}, and 6 nm, respectively, and the number density of Fe_3O_4 NPs per layer was approximately 2.38×10^{12} cm^{-2}. These results imply that OA–Fe_3O_4 NPs are densely packed within the films. In addition, the thickness of the (OA–Fe_3O_4 NP)$_n$ multilayer film increased from approximately 22 to 147 nm, which indicates that the thickness of one layer almost equaled the diameter of a single OA–Fe_3O_4 NP (approximately 6 nm) when the number of layers (n) was increased from 2 to 15 (Fig. 2c). Although the photo-crosslinked Fe_3O_4 NP film of about 81 nm thickness can be prepared by single-step spin coating using a low spinning speed of 500 rpm and a high solution concentration of 30 mg mL^{-1}, the surface of a single-step spin-coated film was much rougher compared to that of (OA–Fe_3O_4 NP)$_8$ films

prepared using a spinning speed of 3000 rpm and a solution concentration of 5 mg mL^{-1}. As a result, the root-mean-square (rms) roughnesses of single-step and multilayered films were measured to be about 17.0 nm and 2.4 nm, respectively, despite their similar thicknesses. In the case of the single-step spin-coated OA–Fe_3O_4 film with 30 mg mL^{-1} at 3000 rpm, the film thickness and the root-mean-square roughness were measured to be about 42 nm and 8.064 nm. However, for the (OA–Fe_3O_4 NP)$_4$ multilayer film with 5 mg mL^{-1} and 3000 rpm, those were 45 nm and 2.528 (see ESI, Table S1 and Fig. S1†).

The internal structure of the photo-crosslinked (OA–Fe_3O_4 NP)$_{20}$ multilayered film was examined by cross-sectional high-resolution transmission electron microscopy (HR-TEM). As shown in Fig. 2d, OA–Fe_3O_4 NPs are homogeneously but densely distributed within the films without any NP segregation. These phenomena contrast sharply with previous reports that organic/inorganic multilayers based on photo-crosslinkable polymers exhibited a stratified internal structure due to the segregation of polymer-encapsulated NPs during spin-coating.[36,41] A variety of inorganic NPs, such as Ag, MnO, and FePt, as well as Fe_3O_4, can also be easily LbL assembled using a photoinitiator (see ESI, Fig. S2–S4†). From a practical viewpoint, the uniform distribution and dense packing of NPs are very important properties with respect to their use in electronic devices such as NP-based memory devices because uniformly distributed and densely packed NPs would possibly allow for a smaller chip size and electron tunneling between neighboring NPs. More details will be discussed in the later part of this study. On the other hand, the spin-coating of the solution mixture containing OA–Fe_3O_4 NPs, PI and hydrophobic polymer such as polystyrene induced the two distinct layers (*i.e.*, polymer and OA–Fe_3O_4 NP layer) because of the segregation phenomenon by their unfavorable interfacial interaction (see ESI, Fig. S5†).[36]

First, the magnetic properties of the photo-crosslinked (OA–Fe_3O_4 NP)$_n$ ($n = 5$ and 15) multilayer films were investigated by superconducting quantum interference device (SQUID) magnetometry in the field range of −5000 to +5000 Oe. The magnetization curves of the crosslinked multilayers measured at $T = 300$ K were reversible without coercivity, remanence, or hysteresis, which implies superparamagnetic behavior (Fig. 3a).[42,43] However, at liquid helium temperature ($T = 5$ K), the thermally activated magnetization flipping properties of the Fe_3O_4 NPs revealed frustrated superparamagnetic properties; *i.e.*, the magnetization curves assumed a loop shape with distinct separation of the two sweeping directions, which is typically observed with ferromagnets (Fig. 3b). In addition, the saturated magnetization increased regularly with the number of bilayers (*i.e.*, the total amount of OA–Fe_3O_4 NPs adsorbed within the multilayer films) (Fig. 3a and b). Fig. 3c shows the temperature dependence of the magnetization of the resulting photo-crosslinked (OA–Fe_3O_4 NP)$_n$ films from 300 to 5 K under an applied magnetic field of 150 Oe. The blocking temperature, which began to show some deviation between zero-field-cooled (ZFC) and field-cooled (FC) magnetization,[42,44] was fixed at approximately 45 K for 5 and 15 multilayered films. Although it was reported that the blocking temperature of a Fe_3O_4 NP array was shifted to significantly higher temperatures in a 3D NP

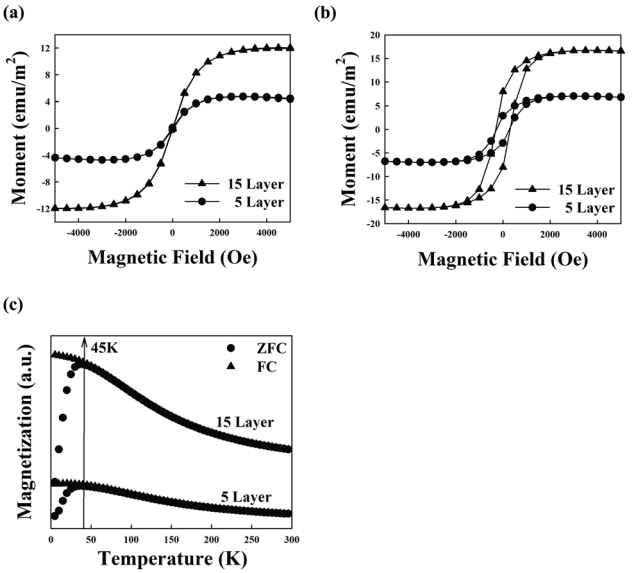

Fig. 3 The magnetic curves of (photo-crosslinked OA–Fe_3O_4 NP)$_{n=5,\ and\ 15}$ multilayers films at (a) 300 and (b) 5 K. (c) Temperature dependence of zero-field cooling (ZFC) and field cooling (FC) magnetization measured using 150 Oe.

array because of the relatively strong dipole interactions between the magnetic moments of the individual particles,[45] our results evidently show that the densely packed iron oxide NP films can maintain the inherent superparamagnetic properties of their component NPs.

Other authors have reported that Fe_3O_4 nanoparticles with sizes less than 10 nm showed relatively high resistivity (>50 MΩ cm) due to the nanosize effect when pressed into compact pellets.[46] Although they suggested that the

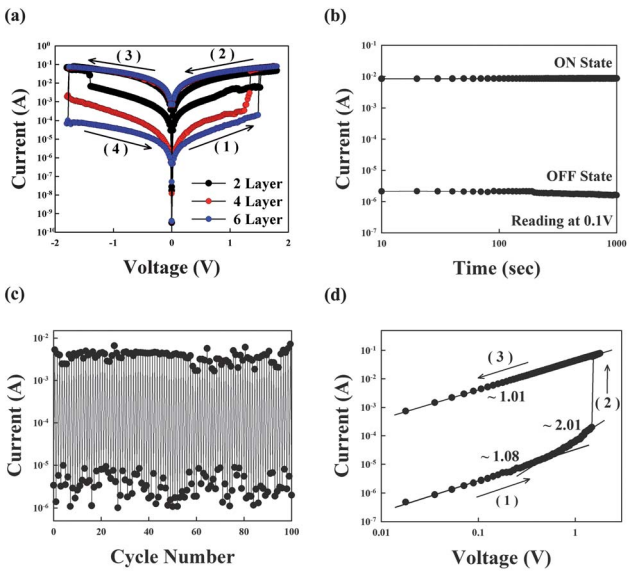

Fig. 4 (a) *I–V* curves of the (photo-crosslinked OA–Fe_3O_4 NP)$_{n=2,4\ and\ 6}$ multilayered device. (b) Retention time and (c) cycling test of the (photo-crosslinked OA–Fe_3O_4 NP)$_{n=6}$ multilayered device at a reading voltage of 0.1 V. (d) The linear fitting for the *I–V* curve of 6 bilayered devices on a log–log scale during a positive voltage sweep.

nanoparticle pellets exhibited bipolar switching properties according to the voltage polarity, their results were strongly influenced by faulty fluctuations in their instrument. Fig. 4a shows the nonvolatile memory properties of the (cross-linked OA–Fe_3O_4 NP)$_n$ multilayer films. For measurements of bipolar switching, the voltage was swept from 0 to 1.8 V and then back to −1.8 V with limited current compliance up to 100 mA. More specifically, the low-current state (*i.e.*, the OFF state) [step '(1)'] was suddenly converted to a high-current state (*i.e.*, the ON state) at +1.5 V. When the polarity of the voltage applied to the (crosslinked Fe_3O_4 NP)$_n$ multilayer film was reversed at +1.8 V [step '(2)'], the ON state was maintained from +1.8 to −1.8 V and then converted to the low-current state at −1.8 V.

The increase in the number of layers resulted in a notably lower current level, especially the OFF level, because the electric field across the (crosslinked Fe_3O_4 NP)$_n$ multilayer films decreased when the number of layers was increased from 2 to 6 (Fig. 4a). As a result, the ON/OFF current ratio of these devices was increased to approximately 10^3. It should be noted that this device performance can be further improved with increasing number of layers (see ESI, Fig. S6†).

To further investigate the stability of the resistive switching properties of transition metal oxide NP-based devices, cycling and retention time tests of (crosslinked Fe_3O_4 NP)$_6$ multilayer devices were performed to determine their electrical stability in the ON and OFF states using a reading voltage of +0.1 V. Fig. 4b and c show that the ON and OFF states remained stable during the entire test period of 10^3 s and 100 cycles were performed under ambient air conditions. The ratio of the current in the ON state to that in the OFF state was approximately 10^3, and these devices were operated repeatedly at a switching speed of 640 μs. The memory performance of (crosslinked Fe_3O_4 NP)$_n$ multilayer films was achieved without any thermal treatment of the films after they were prepared.

To investigate the conduction mechanism of the (crosslinked Fe_3O_4 NP)$_n$ multilayer films, the nonlinear *I*–*V* characteristics in the positive voltage sweep region were plotted on a log–log scale. Fig. 4d shows that the *I*–*V* relationship in the ON state clearly exhibited charge transport behavior, which was similar to that of space-charge-limited conduction (SCLC).[47,48] The SCLC model is composed of an ohmic current region ($I \propto V$) because of thermally generated charge carriers, a Mott–Gurney law region (also known as Child's law in solids) ($I \propto V^2$), and a region of sharp current increase. In contrast, the ON state showed ohmic conduction behavior with a slope of 1.00. In this case, the ON current might flow through a local conduction path, such as a metallic filament that acts as a resistor with low resistivity. To confirm the formation of a conduction path within Fe_3O_4 NP-based films, local current images were monitored by current-sensing atomic force microscopy (CS-AFM).[49–51] In these measurements, the CS-AFM tip (*i.e.*, an electrochemically inert Pt tip) with a contact area of approximately 30 nm was used as the top electrode.

As shown in Fig. 5, the formation and rupture of filamentary conductive paths were observed in both the ON and OFF states, as indicated in the *I*–*V* curve of a cross-linked OA–Fe_3O_4 NP film. These phenomena show that the current densities between the top and bottom electrodes were not uniform; they were concentrated in localized conductive paths that were turned on and off during switching. The relatively low conductivity and high operating voltages shown in the CS-AFM data compared to those measured from 50 μm sized top electrodes (see Fig. 4a) are mainly caused by the decrease in the electrode contact area. A decrease in electrode contact area has been reported to decrease the density of conductive filamentary paths formed under a top electrode and to consequently increase the operating voltage.[51] The CS-AFM tip, because of its small contact area (approximately 30 nm), may also function as an electrical point source, thereby causing the electric field exerted from the tip throughout the crosslinked OA–Fe_3O_4 films to be non-uniform. A non-uniform electric field is known to increase the applied voltages for resistive switching.[49]

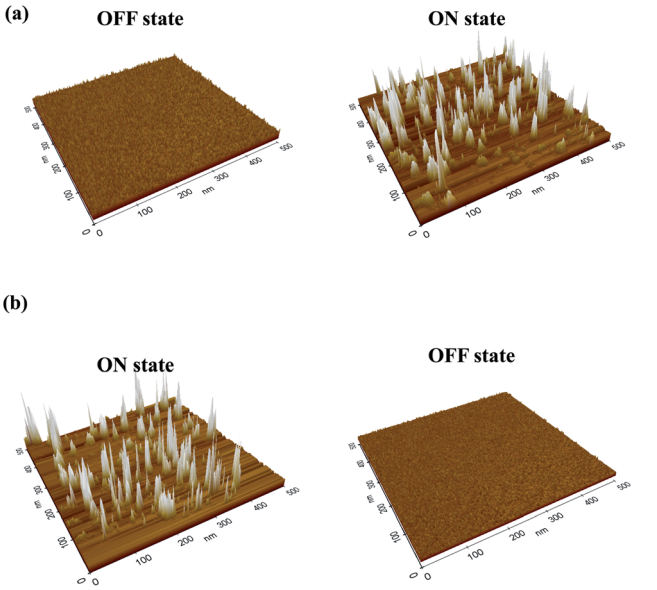

Fig. 5 CS-AFM images of the (crosslinked OA–Fe_3O_4)$_1$ multilayers in (a) OFF (∼+0.2 V) and ON state (∼+5 V) during positive voltage sweep, and (b) ON (∼−5 V) and OFF (∼−0.2) state during negative voltage sweep. CS-AFM images of multilayer devices were measured from the respective regions in the *I*–*V* curve of the (crosslinked OA–Fe_3O_4)$_2$ multilayers device. The formation of conductive filamentary paths was confirmed by CS-AFM characterizations. In this case, the electrochemically inert Pt tip was used as a top electrode instead of Ag electrode. The formation and rupture of the randomly distributed paths were observed after "SET" processes (*i.e.*, switching from low current (OFF) to high current (ON) state) and "RESET" (*i.e.*, switching from high current (ON) to low current (OFF) state).

Furthermore, we investigated the possibility that one bare OA–Fe_3O_4 NP without any coated PI could be operated as a nano-scale memory device (Fig. 6). For this investigation, OA–Fe_3O_4 NP-coated substrates were prepared onto Pt-coated Si substrates using OA–Fe_3O_4 solution with extremely diluted concentration (<1×10^{-4} mg mL^{-1}). In this case, the nonvolatile memory properties of one OA–Fe3O4 NP in an area of 16 × 16 nm^2 was measured using a CS-AFM tip electrode with a current compliance of 1.0 μA. As shown in Fig. 6, one OA–Fe_3O_4 NP displayed the typical bipolar switching behavior.

Although the switching mechanism in transition metal oxide NP-based devices is unclear, a possible mechanism of the resistive switching behavior in our system can be explained on

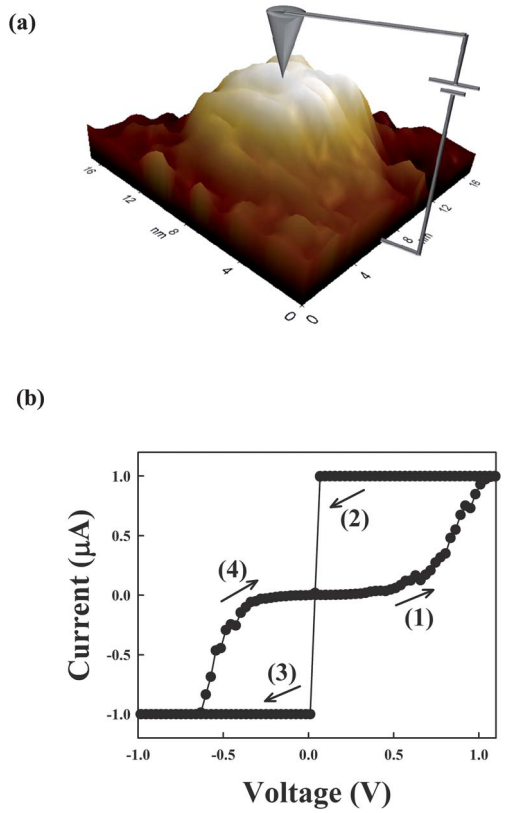

Fig. 6 (a) Schematic and (b) *I–V* curve of one bare OA–Fe_3O_4 NP measured from CS-AFM with a current compliance of 1.0 μA.

the basis of the memristive model.[51,52] The positively charged carriers (*i.e.*, Fe ions) in the Fe_3O_4 NP lattices are repelled by or attracted to the top electrode according to the electric field and can drift as a result of tunneling through a thin residual region (*i.e.*, the undoped charge-carrier region within Fe_3O_4 NP and organic layers, including OA ligands and PI). As previously mentioned, photo-crosslinked multilayers are composed of densely packed Fe_3O_4 NPs. This charge drift has a significant effect on the electronic barrier to electron transport at the interface between the electrode and the multilayers; *i.e.*, a positive voltage applied to the top electrode repels positively charged carriers in the Fe_3O_4 NP lattices, thereby inducing a low-conductivity (*i.e.*, OFF) state due to the large energy barrier between the top electrode and the Fe_3O_4 NPs. This low current state was suddenly converted into the high current state when the positively charged carriers were sufficiently accumulated into the bottom electrode. However, when a voltage with reverse polarity is applied to the top electrode, the positively charged carriers are attracted to the top interface, and these charges drift in the electric field through the most favorable diffusion paths to form channels with high electrical conductivity.

Solid electrolytes sandwiched between an electrochemically active (Ag or Cu) anode and an inert cathode have recently been reported to induce bipolar switching behavior *via* an electrochemical redox reaction based on the high mobility of Ag ions, which may represent another switching mechanism.[48,53–55] Furthermore, metal–ion diffusion from the top electrode can result in the formation of localized metal–atom chains that bridge the electrode materials under an electric field. However, our device showed bipolar switching behavior from an electrochemically inert tungsten top electrode and a Pt electrode. Furthermore, bipolar switching behavior similar to that shown in Fig. 4a was observed from a variety of top electrode materials (see ESI, Fig. S7†). These results imply that the redox reaction based on the metal ions diffused from the top electrode is not directly related to the resistive switching behavior of photo-crosslinked (OA–Fe_3O_4 NP)$_n$ multilayers, even though the process may be partially assisted.

For more evidently demonstrating the effectiveness of photo-crosslinking LbL-assembly, we prepared the memory cell devices with patterned electrodes using photo-crosslinkable Ag NPs without any aid of vacuum deposition. First, the (crosslinked OA–Fe_3O_4 NP)$_6$ multilayer film was deposited onto a Pt-coated substrate, and then the solution mixture of 3 wt% OA–Ag NPs with a diameter of 6.5 nm and PI was successively spin-coated onto the OA–Fe_3O_4 NP multilayers. After spin-coating of OA–Ag NPs, the UV light was irradiated onto the films using a photomask with 100 μm sized dot patterns, and then the unirradiated OA–Ag NP region was removed using the toluene washing solvent. These cell devices with patterned OA–Ag NPs were dried at 120 °C (Fig. 7a and ESI, Scheme S1†). In this case, it was confirmed that the bipolar switching properties of photo-patterned devices were almost similar to those of devices shown in Fig. 7b. Although the vacuum deposition of top electrodes onto the nanoporous thin film such as OA–Fe_3O_4 NP films often gives rise to the short circuit current phenomenon (see ESI,

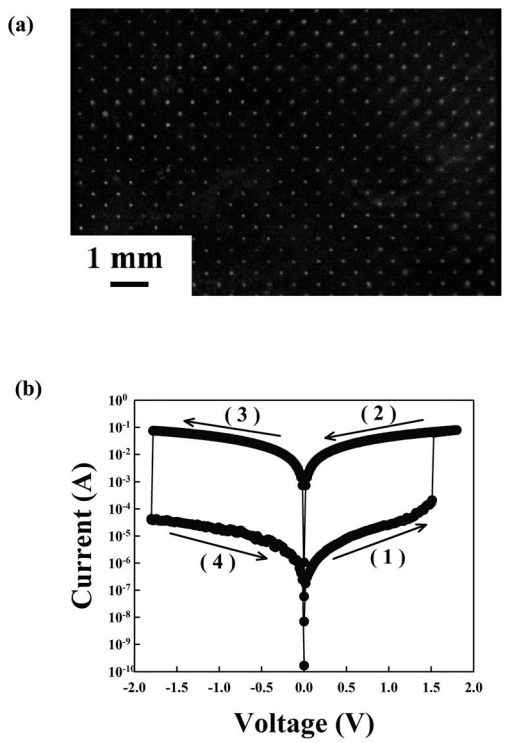

Fig. 7 (a) Optical image of patterned Ag electrode deposited through photo-crosslinking LbL-assembly on the (crosslinked OA–Fe_3O_4 NP)$_6$ multilayer film and (b) the bipolar switching properties of photo-patterned devices.

Fig. S8†), our approach significantly reduced the short circuit current phenomenon causing the electrical malfunction.

4. Conclusion

We have demonstrated that nanocomposite multilayer films composed of functional inorganic NPs can be easily prepared by a photo-crosslinking LbL-assembly approach. The present strategy is that hydrophobic inorganic NPs with desirable qualities (*i.e.*, uniform size and high crystallinity) synthesized in organic media can be directly incorporated into LbL-assembled films without any additional surface modification of the pristine NPs. The crosslinking reaction between OA ligands bound to the surface of NPs and PI molecules with low M_w (approximately 204.3 g mol^{-1}) induced the formation of homogeneously and densely packed NP layers within films. We also demonstrated that our approach could be applied to a variety of NPs that range from metals to transition metal oxides. Furthermore, nonvolatile memory devices prepared from photo-crosslinked Fe_3O_4 NP multilayers and Ag NP electrodes exhibited reversible resistive switching properties, with an ON/OFF current ratio of above 10^3, and appreciable device stability despite the use of room-temperature processes.

Acknowledgements

This work was supported by the National Research Foundation (NRF) grant funded by the Korea government (MEST) (2010-0029106) and by the Human Resources Development Program of KETEP grant (No. 20114010203050) funded by the Korea government Ministry of Trade, Industry and Energy.

Notes and references

1 Y. Xiao, F. Patolsky, E. Katz, J. F. Hainfeld and I. Willner, *Science*, 2003, **299**, 1877–1881.
2 A. M. Yu, Z. J. Liang, J. Cho and F. Caruso, *Nano Lett.*, 2003, **3**, 1203–1207.
3 K. Mohanta, S. K. Majee, S. K. Batabyal and A. J. Pal, *J. Phys. Chem. B*, 2006, **110**, 18231–18235.
4 J. S. Lee, J. Cho, C. Lee, I. Kim, J. Park, Y. M. Kim, H. Shin, J. Lee and F. Caruso, *Nat. Nanotechnol.*, 2007, **2**, 790–795.
5 P. Podsiadlo, A. K. Kaushik, E. M. Arruda, A. M. Waas, B. S. Shim, J. D. Xu, H. Nandivada, B. G. Pumplin, J. Lahann, A. Ramamoorthy and N. A. Kotov, *Science*, 2007, **318**, 80–83.
6 Y. Du, L. E. Luna, W. S. Tan, M. F. Rubner and R. E. Cohen, *ACS Nano*, 2010, **4**, 4308–4316.
7 S. W. Lee, J. Kim, S. Chen, P. T. Hammond and Y. Shao-Horn, *ACS Nano*, 2010, **4**, 3889–3896.
8 K. M. Holder, M. A. Priolo, K. E. Secrist, S. M. Greenlee, A. J. Nolte and J. C. Grunlan, *J. Phys. Chem. C*, 2012, **116**, 19851–19856.
9 K. H. Kim, J. H. Moon, E. Y. Kim, H. J. Kim, S. H. Jang and W. I. Lee, *J. Mater. Chem.*, 2012, **22**, 11179–11184.
10 Y. Wei, H. Liu, Y. Jin, K. Cai, H. Li, Y. Liu, Z. Kang and Q. Zhang, *New J. Chem.*, 2013, **37**, 886–889.
11 J. Y. Ouyang, C. W. Chu, C. R. Szmanda, L. P. Ma and Y. Yang, *Nat. Mater.*, 2004, **3**, 918–922.
12 L. C. Hu, Y. Yonamine, S. H. Lee, W. E. van der Veer and K. J. Shea, *J. Am. Chem. Soc.*, 2012, **134**, 11072–11075.
13 B. J. Kim, J. Bang, C. J. Hawker, J. J. Chiu, D. J. Pine, S. G. Jang, S. M. Yang and E. J. Kramer, *Langmuir*, 2007, **23**, 12693–12703.
14 A. K. Boal, F. Ilhan, J. E. DeRouchey, T. Thurn-Albrecht, T. P. Russell and V. M. Rotello, *Nature*, 2000, **404**, 746–748.
15 S. B. Roscoe, S. Yitzchaik, A. K. Kakkar, T. J. Marks, Z. Y. Xu, T. G. Zhang, W. P. Lin and G. K. Wong, *Langmuir*, 1996, **12**, 5338–5349.
16 G. Decher, *Science*, 1997, **277**, 1232–1237.
17 F. Caruso, R. A. Caruso and H. Mohwald, *Science*, 1998, **282**, 1111–1114.
18 J. S. Major and G. J. Blanchard, *Chem. Mater.*, 2002, **14**, 2574–2581.
19 T. C. Wang, R. E. Cohen and M. F. Rubner, *Adv. Mater.*, 2002, **14**, 1534–1537.
20 J. Cho, J. F. Quinn and F. Caruso, *J. Am. Chem. Soc.*, 2004, **126**, 2270–2271.
21 N. Zhao, F. Shi, Z. Q. Wang and X. Zhang, *Langmuir*, 2005, **21**, 4713–4716.
22 J. Cho, J. K. Hong, K. Char and F. Caruso, *J. Am. Chem. Soc.*, 2006, **128**, 9935–9942.
23 G. K. Such, J. F. Quinn, A. Quinn, E. Tjipto and F. Caruso, *J. Am. Chem. Soc.*, 2006, **128**, 9318–9319.
24 K. Wen, R. Maoz, H. Cohen, J. Sagiv, A. Gibaud, A. Desert and B. M. Ocko, *ACS Nano*, 2008, **2**, 579–599.
25 B. Lee, Y. Kim, S. Lee, Y. S. Kim, D. Wang and J. Cho, *Angew. Chem., Int. Ed.*, 2010, **49**, 359–363.
26 Y. Ko, Y. Kim, H. Baek and J. Cho, *ACS Nano*, 2011, **5**, 9918–9926.
27 M. Yoon, Y. Kim and J. Cho, *ACS Nano*, 2011, **5**, 5417–5426.
28 Y. H. Kim, Y. M. Lee, J. Y. Lee, M. J. Ko and P. J. Yoo, *ACS Nano*, 2012, **6**, 1082–1093.
29 O. Crespo-Biel, B. Dordi, D. N. Reinhoudt and J. Huskens, *J. Am. Chem. Soc.*, 2005, **127**, 7594–7600.
30 F. Zhang and M. P. Srinivasan, *Langmuir*, 2007, **23**, 10102–10108.
31 Y. Kim, C. Lee, I. Shim, D. Wang and J. Cho, *Adv. Mater.*, 2010, **22**, 5140–5144.
32 K. C. Grabar, K. J. Allison, B. E. Baker, R. M. Bright, K. R. Brown, R. G. Freeman, A. P. Fox, C. D. Keating, M. D. Musick and M. J. Natan, *Langmuir*, 1996, **12**, 2353–2361.
33 J. Schmitt, G. Decher, W. J. Dressick, S. L. Brandow, R. E. Geer, R. Shashidhar and J. M. Calvert, *Adv. Mater.*, 1997, **9**, 61–65.
34 S. H. Sun, H. Zeng, D. B. Robinson, S. Raoux, P. M. Rice, S. X. Wang and G. X. Li, *J. Am. Chem. Soc.*, 2004, **126**, 273–279.
35 S. H. Sun, *Adv. Mater.*, 2006, **18**, 393–403.
36 S. Lee, B. Lee, B. J. Kim, J. Park, M. Yoo, W. K. Bae, K. Char, C. J. Hawker, J. Bang and J. Cho, *J. Am. Chem. Soc.*, 2009, **131**, 2579–2587.

37 L. H. Piao, K. H. Lee, W. J. Kwon, S. H. Kim and S. Yoon, *J. Colloid Interface Sci.*, 2009, **334**, 208–211.
38 H. B. Na, J. H. Lee, K. J. An, Y. I. Park, M. Park, I. S. Lee, D. H. Nam, S. T. Kim, S. H. Kim, S. W. Kim, K. H. Lim, K. S. Kim, S. O. Kim and T. Hyeon, *Angew. Chem., Int. Ed.*, 2007, **46**, 5397–5401.
39 M. Chen, J. Kim, J. P. Liu, H. Y. Fan and S. H. Sun, *J. Am. Chem. Soc.*, 2006, **128**, 7132–7133.
40 D. A. Buttry, *Applications of the Quartz Crystal Microbalance to Electrochemistry*, Dekker, New York, 1991.
41 S. Al Akhrass, F. Gal, D. Damiron, P. Alcouffe, C. J. Hawker, F. Cousin, G. Carrot and E. Drockenmuller, *Soft Matter*, 2009, **5**, 586–592.
42 J. Park, K. J. An, Y. S. Hwang, J. G. Park, H. J. Noh, J. Y. Kim, J. H. Park, N. M. Hwang and T. Hyeon, *Nat. Mater.*, 2004, **3**, 891–895.
43 K. M. Seemann, A. Bauer, J. Kindervater, M. Meyer, C. Besson, M. Luysberg, P. Durkin, W. Pyckhout-Hintzen, N. Budisa, R. Georgii, C. M. Schneider and P. Kogerler, *Nanoscale*, 2013, **5**, 2511–2519.
44 J. Majeed, O. D. Jayakumar, H. G. Salunke, B. P. Mandal, G. Lawes, R. Naik and A. K. Tyagi, *RSC Adv.*, 2013, **3**, 596–602.
45 P. Poddar, T. Telem-Shafir, T. Fried and G. Markovich, *Phys. Rev. B: Condens. Matter Mater. Phys.*, 2002, **66**, 060403.
46 T. H. Kim, E. Y. Jang, N. J. Lee, D. J. Choi, K. J. Lee, J. T. Jang, J. S. Choi, S. H. Moon and J. Cheon, *Nano Lett.*, 2009, **9**, 2229–2233.
47 J. G. Park, W. S. Nam, S. H. Seo, Y. G. Kim, Y. H. Oh, G. S. Lee and U. G. Paik, *Nano Lett.*, 2009, **9**, 1713–1719.
48 Y. C. Yang, F. Pan, Q. Liu, M. Liu and F. Zeng, *Nano Lett.*, 2009, **9**, 1636–1643.
49 H. Sugimura, Y. Ishida, K. Hayashi, O. Takai and N. Nakagiri, *Appl. Phys. Lett.*, 2002, **80**, 1459–1461.
50 C. Lee, I. Kim, H. Shin, S. Kim and J. Cho, *Langmuir*, 2009, **25**, 11276–11281.
51 H. Baek, C. Lee, J. Choi and J. Cho, *Langmuir*, 2013, **29**, 380–386.
52 D. B. Strukov, G. S. Snider, D. R. Stewart and R. S. Williams, *Nature*, 2008, **453**, 80–83.
53 J. J. Yang, M. D. Pickett, X. Li, A. A. OhlbergDouglas, D. R. Stewart and R. S. Williams, *Nat. Nanotechnol.*, 2008, **3**, 429–433.
54 K. Terabe, T. Hasegawa, T. Nakayama and M. Aono, *Nature*, 2005, **433**, 47–50.
55 R. Waser and M. Aono, *Nat. Mater.*, 2007, **6**, 833–840.

